.

Ionic adsorption on the brucite (0001) surface: A periodic electrostatic embedded cluster method study

Eszter Makkos, Andrew Kerridge, Jonathan Austin, and Nikolas Kaltsoyannis

Ionic adsorption on the brucite (0001) surface: A periodic electrostatic embedded cluster method study

Eszter Makkos,[1] Andrew Kerridge,[1,2] Jonathan Austin,[3] and Nikolas Kaltsoyannis[1,4,a)]

[1]*Department of Chemistry, University College London, 20 Gordon Street, London WC1H 0AJ, United Kingdom*
[2]*Department of Chemistry, Lancaster University, Bailrigg, Lancaster LA1 4YB, United Kingdom*
[3]*National Nuclear Laboratory, Chadwick House, Birchwood Park, Warrington WA3 6AE, United Kingdom*
[4]*School of Chemistry, The University of Manchester, Manchester M13 9PL, United Kingdom*

Density functional theory (DFT) at the generalised gradient approximation level is employed within the periodic electrostatic embedded cluster method (PEECM) to model the brucite (0001) surface. Three representative studies are then used to demonstrate the reliability of the PEECM for the description of the interactions of various ionic species with the layered $Mg(OH)_2$ structure, and its performance is compared with periodic DFT, an approach known to be challenging for the adsorption of charged species. The adsorption energies of a series of s block cations, including Sr^{2+} and Cs^+ which are known to coexist with brucite in nuclear waste storage ponds, are well described by the embedded cluster model, provided that basis sets of triple-zeta quality are employed for the adsorbates. The substitution energies of Ca^{2+} and Sr^{2+} into brucite obtained with the PEECM are very similar to periodic DFT results, and comparison of the approaches indicates that two brucite layers in the quantum mechanical part of the PEECM are sufficient to describe the substitution. Finally, a detailed comparison of the periodic and PEECM DFT approaches to the energetic and geometric properties of differently coordinated $Sr[(OH)_2(H_2O)_4]$ complexes on brucite shows an excellent agreement in adsorption energies, Sr–O distances, and bond critical point electron densities (obtained via the quantum theory of atoms-in-molecules), demonstrating that the PEECM can be a useful alternative to periodic DFT in these situations. *Published by AIP Publishing.* [http://dx.doi.org/10.1063/1.4968035]

I. INTRODUCTION

Modelling ionic sorption mechanisms on surfaces is the key to understanding a wide range of physical phenomena in catalytic chemistry,[1–5] biochemistry,[6,7] energy storage,[8,9] and environmental chemistry, where modelling has been used to study the migration of ion contaminants in soils and sediments[10–16] and the treatment of polluted water with adsorbent materials.[17–19] Computational studies can provide insight into ion/surface interactions at the molecular level by predicting preferred reaction sites,[2,4,5,14,17] calculating the most stable structures during the interactions[1,9,14,19] and allowing the comparison of the interaction energies of competing species.[15,18,20]

However, choosing a suitable surface representation for the investigation of a particular adsorption mechanism is not always straightforward, and the choice can heavily influence the outcome of the results. By far the most common approach to model surfaces is periodic density functional theory (DFT),[21] which operates with conventional unit cells and employs periodic boundary conditions. However, modelling charged systems using periodic boundary conditions is extremely difficult[9,22,23] and is often avoided by including counter ions in the simulation box.[9,20] Furthermore, large super cells are often required to study

isolated interaction sites,[24–26] which significantly increases the computational cost.

One alternative to modelling a surface with periodic DFT is to use isolated molecular clusters to represent the adsorption site of the surface. This approach has been used mainly for 2D materials, such as graphene,[18] where the far-field effects of the substrate on the adsorption reaction can be neglected, i.e., the interaction is very localised.

For adsorption on ionic crystals, embedded cluster methods are commonly used as an alternative to periodic DFT.[24,27,28] These approaches have the advantage of being able to study isolated adsorption sites and can deal with charged systems with levels of theory beyond the generalised gradient approximation (GGA) methods, typical of periodic DFT calculations. This last feature is especially useful for systems such as metal oxides and oxygen defects of metal oxides, where hybrid functionals are necessary for the accurate description of the electronic structure.[22,27,29,30] One such technique is the periodic electrostatic embedded cluster method (PEECM)[27,31] which features a quantum mechanically treated region (the QM cluster) embedded in an infinite periodic array of point charges (PCs). This approach provides an accurate description of the long range electrostatic interactions between the ionic crystal and the adsorption site by calculating the corresponding electrostatic potential via the periodic fast multipole method.[32] A region intermediate between the QM cluster and the PCs is often necessary to prevent artificial over-polarisation of the former due to

---
a)Author to whom correspondence should be addressed. Electronic address: nikolas.kaltsoyannis@manchester.ac.uk

the neighbouring positive charges in the latter.[31] The most common type of intermediate region represents the positive ions with softening effective core potentials and the negative ions with formal charges.[24,27,29]

The first generation of British civil nuclear power reactors used a Mg–Al alloy, called Magnox, as a fuel cladding.[33] Much of this cladding (along with spent uranium oxide fuel) is currently stored in legacy ponds and silos, most notably in Sellafield, and has corroded to form heterogeneous sludges consisting mainly of brucite ($Mg(OH)_2$), along with other Mg-based minerals and uranium oxides.[34] The aqueous phase in the ponds contains a range of soluble radioisotopes, from which the biggest contributors to radioactivity are ^{137}Cs and ^{90}Sr.[35] Since there is only limited access to real samples and monitoring the conditions *in situ* is difficult (due to the radiation hazards), computational modelling can play an important role in understanding the behaviour of the radioactive ions in the ponds and the environment, thus informing improvements in the waste treatment processes. There are several examples in the literature in which simulations have helped to improve our knowledge of radionuclide-related transport mechanisms in minerals[36] by determining the strength and type of their interaction with transport media, such as molecular dynamics studies of the interaction of solvated uranyl ions with common soil components around nuclear waste depositaries,[11,13,14,37,38] and computational investigations of ionic transport mechanisms in the filtration media used during the decommissioning process such as sand and zeolite type ion exchangers.[39,40]

Brucite contains layers of $Mg(OH)_2$, where the hydroxyl groups are orthogonal to the hexagonal basal plane (space group D^3_{3d}, P3m1). The bulk structure of this material is well understood from previous experimental[41,42] and computational studies.[43–50] The interlayer distance is rather large due to the weak interlayer forces. Although some experimental results suggest a degree of hydrogen bonding between the layers,[51,52] the majority of previous studies predict only weak dispersion type forces,[45,49,53] indicating that it is easy to cleave the structure. Theoretical studies agree that employing GGA or hybrid functionals for the crystal structure optimisation gives bulk geometrical parameters in good agreement with the experiment[45–47,49] but slightly underestimates the interaction energies between the $Mg(OH)_2$ layers.[46,47] Applying dispersion corrections with a hybrid functional gives a slightly better estimation for the strength of the interlayer attraction[48] but predicts the interlayer distance to be shorter than the experimental value.

Based on the Wulff construction method,[54] transmission electron microscopy, and X-ray diffraction studies,[55] it is known that the brucite crystal forms in a hexagonal prismatic structure with (0001) and (1$\bar{1}$00) surfaces. The most stable and abundant face is the (0001) in which the hydroxide ions surround the magnesium ion in an octahedral coordination, resulting in a hexagonal ordered Mg^{2+} with the OH groups facing outwards.

We have previously identified computationally the most stable hydrate[56] and hydroxide[57,58] complexes of Sr^{2+} in an aqueous solution and here move on to develop an efficient model for studying the adsorption of Sr^{2+} complexes on the hydrated (0001) brucite surface, using the PEECM, which has

previously been employed to study ionic materials.[24,27] Electronic structure calculations[44] as well as Mulliken population analysis[46] predict largely the ionic character for the Mg–O bond but more covalent character for the O–H bond. This feature of the material allows us to employ embedded methods as for an ordinary metal oxide, as we define the QM cluster without cutting covalent bonds at the boundaries. Although there are a small number of examples for similar embedded calculations,[59,60] to the best of our knowledge, this is the first time a surface of a not purely ionic material has been modelled with the PEECM.

Our paper is structured as follows. Sections II A and II B provide a detailed description of our computational surface models using the PEECM, and also our periodic DFT studies which we report for comparative purposes. Section III A then presents a study of single ion adsorption using the developed embedded surface model in which we compare the adsorption energies of different s block ions and test the effect of using different basis sets on the relative adsorption energies. In Sections III B and III C we show through two model cases that the embedded cluster model gives similar results for neutral systems as does periodic DFT and, by studying the effect of cell size with periodic DFT, we derive conclusions about the required size of the QM cluster.

II. COMPUTATIONAL DETAILS

A. PEECM model

All calculations were performed with version 6.6 of the TURBOMOLE program[61] using resolution-of-the-identity density functional theory.[62] Results were visualised with the MOLDRAW chemical graphical software.[63] The TPSS exchange-correlation functional, which employs the meta-generalised gradient approximation (meta-GGA),[64] was used as it has been shown to describe Sr^{2+} complexes well in the past[56] and previous theoretical studies on brucite have shown that GGA functionals efficiently describe bulk properties.[45–47] The brucite surface was considered as a slab containing 1 or 2 layers of $Mg(OH)_2$ and modelled using the PEECM. In this approach, a finite sized cluster of brucite was treated quantum chemically and embedded in a 2D infinite array of point charges (PCs) (aperiodic in the z direction). The cluster was formed from a stoichiometric 6×6 Mg atom unit cell ($Mg_{36}(OH)_{72}$) per layer of brucite, for which we use the following notation from now on: "***n***×***n*_*m***," where ***n*** is the number of Mg atoms in the x and y directions and ***m*** is the number of brucite layers explicitly included in the cluster. The following surface representations were considered: a single layer (***6×6_1***) in which a $Mg_{36}(OH)_{72}$ sized cluster was embedded, a double layer containing only point charges in the second layer (***6×6_1+PC***), and a double layer in which the second layer has the same sized explicit cluster of brucite as the first (***6×6_2***, $2 \times Mg_{36}(OH)_{72}$). Due to the large size of the QM cluster, def2-SVP basis sets of polarised double-ζ quality (SVP, split valence with polarisation functions)[65,66] were used for all QM atoms. Partial geometry optimisations, in which the boundary atoms of the cluster were held fixed and the inner atoms allowed to fully relax (see Figure 1),[67] were carried out in the gas phase, with the m4 integration grid and the default

convergence criteria: SCF energy: 10^{-6} a.u., structural energy: 10^{-6} a.u., and energy gradient: 10^{-3} a.u.

Experimental cell parameters, obtained via neutron diffraction measurements by Catti *et al.*,[41] were used to define both the initial geometry for the QM cluster and the positions of the PCs in the infinite two dimensional array: the *a* and *b* lattice parameters of the hexagonal unit cell were 3.15 Å, and the interlayer distance *c* was 4.77 Å.

To best of our knowledge, the PEECM approach has been previously used only for purely ionic materials often with conventional unit cell structures such as TiO_2[24] or CeO_2.[27] For these metal oxides effective core potentials (ECPs) were used on the neighbouring cations around the QM cluster to soften the effect of polarisation from the positive charges, as discussed in the Introduction, while formal charges were used on the corresponding anions. By contrast to these examples, brucite has a layered structure, in which the covalently bonded OH group carries a -1 charge. In this case, the use of an ECP region is complicated, in that we do not wish to apportion formal charges to the O and H atoms in the covalently bound OH units. Therefore, to avoid the artificial polarisation effect of neighbouring PCs on the QM cluster, we decided to employ natural charges in the PC region,[68] derived iteratively from the natural population analysis (NPA).[69] Formal charges were used as an initial guess for the embedding array in a single point calculation, from which a new set of NPA charges inside the QM cluster was determined. The values obtained from the centre of the QM cluster were used as charges in the PC region for the following calculation and this step was repeated until no further variation occurred. The following natural charges were obtained through this process: Mg = +1.78, O = −1.33, and H = +0.44. Applying these charges in the partial optimisation resulted in good geometrical agreement with experimental data (see supplementary material, Section 1.1), especially regarding the key features of the surface, such as

FIG. 1. Illustration of the top and side views of the single layer PEECM model (*6×6_1*). The point charges are represented as balls around the QM cluster, the fixed boundary atoms as wires, and the inner part of the cluster as balls and sticks. Bonds between the inside cluster and the boundary atoms are not shown for clarity (Mg = green, O = red, H = grey).

the perpendicular position of the OH groups to the (0001) plane and the planarity of the Mg sites.

For every s block ion investigated in Section III A (Na$^+$, Rb$^+$, Cs$^+$ and Mg^{2+}, Sr^{2+}, Ba^{2+}), the def2-SVP basis set[65,66,70] was used during the geometry optimisation along with the associated effective core potentials[71] for Rb, Cs, Sr, and Ba. The electron density distribution calculations reported in Section III A were performed by generating wavefunction (.wfn) files from the output of the optimisation in TURBOMOLE using the molden2aim program[72] which served as an input for the Multiwfn code.[73] The electron density images were plotted with the VMD[74] visualisation code, using an isosurface value of ±0.0025 a.u.

The Quantum Theory of Atoms-in-Molecules (QTAIM) calculations described in Section III C were performed with the professional version 13.11.04 of AIMAll[75] using the default parameters of the program. The required .wfn files were generated as described above.

B. Periodic DFT model

We chose the CRYSTAL14 code[76,77] to model the brucite (0001) surface with periodic DFT, since this program allows us to use atom-centred basis sets, as used in TURBOMOLE. The TPSS meta-GGA exchange correlation functional, which was used for the development of the PEECM model, is not available in this code. Since TPSS was developed by Perdew and co-workers based on the same philosophy as PBE exchange-correlation functional,[78] we decided to use the latter in CRYSTAL14. PBE is one of the most commonly employed GGA functionals in solid state chemistry, and the GGA level of theory gave good agreement with the experimental parameters of brucite in previous studies.[45–47,49] Following on from the work of Ungliengo *et al.*,[48] we compared the geometrical parameters obtained with PBE to the Grimme type dispersion corrected PBE-D functional.[79,80] Since PBE-D resulted in an interlayer distance 0.15 Å less than the experimental values, we decided to continue with PBE [see the supplementary material, Table (iii)].

Polarised triple-ζ basis sets, derived specifically for solid state calculations by Peintinger *et al.*,[81] were used for the surface atoms (Mg_pob_TZVP_2012, O_pob_TZVP_2012, H_pob_TZVP_2012) along with the Ca atom in the substitution study presented in Section III B (Ca_pob_TZVP_2102). In the case of Sr, the Sr_HAYWSC-311(d11f)G basis set[82] was used for geometry optimisations, whilst single point energies were calculated using doubly polarised triple-ζ basis sets for the valence electrons with the ECP28MWB multi-electron fit quasi-pseudopotential on the electrons of the core 1s-3d orbitals.[71]

Creating starting geometries for the brucite surface in CRYSTAL14 involves several intermediate steps.[83] The results of these calculations are given in the supplementary material, Section 1.2. A full optimisation was performed on the primitive cell of bulk brucite, using a shrinking factor of 8 along with the energy criteria of 10^{-7} a.u. both for the SCF energy convergence and for the geometry optimisation. These parameters gave good agreement of geometrical properties with the experimental values as well as previous computational studies (*a, b* = 3.177 Å and *c* = 4.751 Å). We fixed the
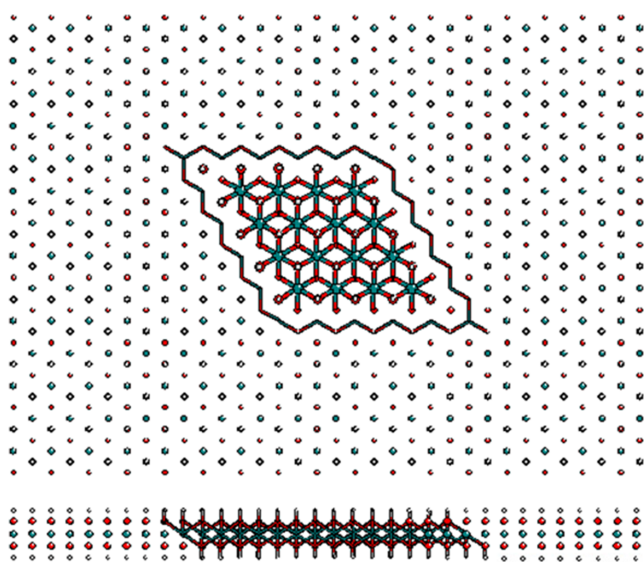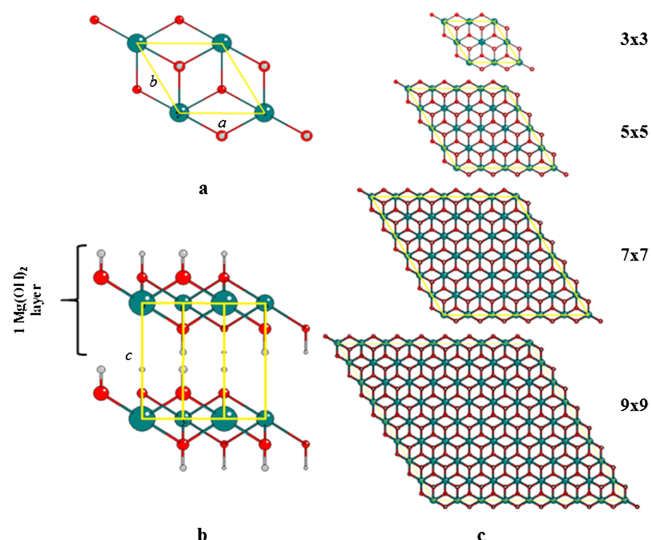
FIG. 2. (a) Top view of the hexagonal unit cell in the brucite crystal structure (a, b are lattice parameters). (b) Side view of the hexagonal unit cell, c is the interlayer distance. 1 $Mg(OH)_2$ layer contains 5 atomic layers. (c) Illustration of the supercells employed (Mg = green, O = red, H = grey).

optimised lattice parameters of the bulk system to create a primitive cell for the (0001) surface and calculated the surface energy along with the Mulliken charges and populations for slabs incorporating different numbers of layers. (One layer of $Mg(OH)_2$ contains 5 atomic layers as shown in Figure 2.) Since, as was discussed in the Introduction, there are only weak dispersion forces between the layers in brucite, including a 2nd layer in the unit cell has only a small effect on the surface energy ($\sim 10^{-6}$ Hartree/m^2), although three layers were required to recover the exact Mulliken charges of the bulk in the middle of the slab.

For the model studies in Sections III B and III C, we created a series of $Mg(OH)_2$ slabs with different supercell sizes (*3×3*, *5×5*, *7×7* and *9×9*) and with 1, 2, and 3 layers of brucite (Figure 2) and optimised the internal coordinates for each using a shrinking factor of 4 along with the convergence criteria: SCF energy: 10^{-7} a.u. and structural energy: 10^{-7} a.u. We used the 0D "MOLECULE" option of CRYSTAL14 for the single point energies of the isolated ions in Section III B and for the solvated $Sr(OH)_2$ complex in Section III C.[84]

For the model studies presented in Sections III B and III C, to make comparison between the two different methods possible, we used the PBE functional with the same computational parameters for the PEECM calculations as was detailed for periodic DFT. Although for the embedded cluster structures def2-SVP basis sets were used for the geometry optimisation, single point energies were obtained after geometry optimisation with the above defined CRYSTAL14 basis functions.

III. RESULTS AND DISCUSSION

In this section, we present the results of three model studies in which we test the reliability of the embedded cluster model developed for the brucite (0001) surface. First, we examine the adsorption of charged systems, by investigating the interaction of a series of s block ions with brucite. Then, we

move on to compare the embedded model calculations with a more widely established method (periodic DFT); we perform a substitution study for single ions into brucite and a second in which we look at the adsorption of differently coordinated $[Sr(OH)_2(H_2O)_4]$ complexes on the surface, comparing their relative stability. We also used the periodic DFT model to carry out cell size studies on the systems of interest and to (indirectly) verify the size of the quantum chemically treated cluster in the PEECM approach.

Note that the adsorption and substitution energies presented in Sections III A and III B are calculated without considering the effects of solvation on the adsorbed or substituted ions. This has been done because the purpose of these calculations is to provide as direct and straightforward a comparison of periodic DFT and PEECM as possible, without the extra variability and complication that will inevitably arise from the treatment of solvation.

A. Single ion adsorption of Sr^{2+} and other s block elements on brucite

We calculated adsorption energies for a series of ions: Na^+, Rb^+, Cs^+ and Mg^{2+}, Sr^{2+}, Ba^{2+} from which Na^+, Cs^+, Sr^{2+}, and Mg^{2+} are known to exist in the aqueous phase in Magnox storage ponds.[35] As described in the Introduction, we have a special interest in $^{90}Sr^{2+}$ and $^{137}Cs^+$, as their adsorption behaviour is especially important in the waste treatment process. We included Rb^+ and Ba^{2+} to make the series of the singly and doubly charged ions more complete, and to allow us to test if the adsorption energies follow the trend expected based on the ionic radii and charges, i.e., the dications should have a stronger interaction with the surface, and the interaction energy should decrease with decreasing ionic charge density.

The following equation was used to calculate the adsorption energies presented in Table I:

$$E_{ads} = E_{complex} - (E_{brucite} + E_{M^{n+}}) \qquad (1)$$

where $E_{complex}$ is the SCF energy of the adsorbed ion with the surface, while $E_{brucite}$ is the energy of the brucite surface model (*6×6_1*, *6×6_1+PC*, or *6×6_2*) and $E_{M^{n+}}$ is the energy of the adsorbed ion. The counterpoise (CP) correction[85] was included to compensate for the artificial energy contribution to the adsorption energy due to the difference in the basis set sizes applied for the components of Eq. (1) (basis set superposition error, BSSE). CP corrected results are shown in brackets in Table I.

The doubly charged ions indeed have a stronger interaction with the surface, the adsorption energy of Mg^{2+}, Sr^{2+}, and Ba^{2+} being almost an order of magnitude stronger (~ 700-1200 kJ/mol) than the adsorption energy of Na^+, Rb^+, and Cs^+ (~ 100 kJ/mol). This difference is probably due to the greater polarisation effect of the dications, as is shown by the electron density difference plots of Sr^{2+} and Cs^+ in Figure 3. Another possibility is the different PEECM electrostatic potential shift of the +1 *vs* +2 systems, though test calculations reveal this to be negligible, <5 kJ/mol. The blue regions in Figure 3 represent electron accumulation while the red areas indicate the electron depletion caused by ion adsorption. Sr^{2+} clearly polarises the oxygen atoms of the brucite cluster much more than Cs^+ does; most likely that is why the Sr^{2+}

TABLE I. Adsorption energies (E_{ads}) of a series of s block ions and relative adsorption energies of different surface representations for a given ion, calculated by comparing the results to the adsorption energy of the **6×6_1** structures (ΔE_{ads}). Counterpoise corrected energy values are presented in brackets (BSSE). (The adsorption energies with ion-SVP and ion-TZVP mixed basis sets were not calculated for **6×6_1+PC**.)

Studied system		E_{ads} (kJ/mol)								ΔE_{ads} (kJ/mol)			
Ion	Layer	def2-SVP	(BSSE)	def2-TZVP	(BSSE)	ion-TZVP	(BSSE)	ion-SVP	(BSSE)	def2-SVP	def2-TZVP	ion-TZVP	ion-SVP
Na$^+$	**6×6_1**	−131.0	(−118.2)	−249.7	(−244.7)	−290.6	(−277.2)	−96.2	(−93.7)	0.0	0.0	0.0	0.0
	+PC	−131.9	(−119.2)	−248.8	(−244.6)	...	...	...	...	−0.9 (−1.1)	0.9 (0.0)	...	...
	6×6_2	−123.6	(−108.4)	−212.1	(−206.7)	−284.0	(−267.4)	−58.8	(−55.9)	7.4 (9.7)	37.6 (38.0)	6.7 (9.8)	37.3 (37.8)
Rb$^+$	**6×6_1**	−144.7	(−136.4)	−112.7	(−108.7)	−149.3	(−138.5)	−110.1	(−106.8)	0.0	0.0	0.0	0.0
	+PC	−144.7	(−136.6)	−110.5	(−106.7)	...	...	...	...	0.1 (0.2)	2.2 (2.0)	...	...
	6×6_2	−135.1	(−124.6)	−76.1	(−71.5)	141.5	(−127.2)	−73.0	(−69.7)	9.6 (11.8)	36.6(37.2)	7.8 (11.4)	37.1 (37.1)
Cs$^+$	**6×6_1**	−118.0	(−109.6)	−94.5	(−91.3)	−127.9	(−119.4)	−85.0	(−82.0)	0.0	0.0	0.0	0.0
	+PC	−117.5	(−109.3)	−92.1	(−89.2)	...	...	...	...	0.5 (0.3)	2.4 (2.2)	...	...
	6×6_2	−108.9	(−98.5)	−57.9	(−54.5)	−119.1	(−108.5)	−48.8	(−45.6)	9.1 (11.1)	36.6(36.9)	8.8 (10.9)	36.2 (36.4)
Mg^{2+}	**6×6_1**	−1182.7	(−1161.4)	−1319.6	(−1311.6)	−1387.0	(−1363.0)	−1123.7	(−1117.7)	0.0	0.0	0.0	0.0
	+PC	−1184.2	(−1168.0)	−1315.6	(−1308.3)	...	...	...	...	−1.5 (−6.6)	4.0 (3.3)	...	...
	6×6_2	−1199.2	(−1178.1)	−1272.5	(−1265.3)	−1404.6	(−1379.9)	−1077.6	(−1072.2)	−16.5 (−16.7)	47.1(46.3)	−17.6 (−16.9)	46.1 (45.5)
Sr^{2+}	**6×6_1**	−890.9	(−874.6)	−835.4	(−828.5)	−901.7	(−882.1)	−825.6	(−819.5)	0.0	0.0	0.0	0.0
	+PC	−895.2	(−880.0)	−834.6	(−828.1)	...	...	...	...	−4.3 (−5.4)	0.8 (0.4)	...	...
	6×6_2	−898.5	(−881.2)	−780.5	(−774.1)	−908.8	(−888.4)	−771.3	(−765.7)	−7.6 (−6.6)	54.9 (54.4)	−7.2 (−6.3)	54.3 (53.8)
Ba^{2+}	**6×6_1**	−717.9	(−702.3)	−730.1	(−721.7)	−793.4	(−777.4)	−653.3	(−647.8)	0.0	0.0	0.0	0.0
	+PC	−722.6	(−707.6)	−729.4	(−723.7)	...	...	...	...	−4.7 (−5.3)	0.7 (−2.0)	...	...
	6×6_2	−723.5	(−706.7)	−674.1	(−665.9)	−798.8	(−781.5)	−598.6	(−591.5)	−5.5(−4.4)	55.9 (55.8)	−5.4 (−4.1)	54.7 (56.3)

binds much more strongly to the surface. Besides showing the different behaviour of the ions, the electron density difference plots also reassure us that there is no artificial polarisation at the edges of the cluster, caused by the false interaction between the charged systems and the point charge region. Furthermore, the images (b) and (d) in Figure 3 suggest only a small contribution from the 2nd layer oxygen atoms to the interaction even in the case of Sr^{2+}.

Examination of the energy trends for the ions of the same charge reveals that, in the case of the monocations, there is a deviation from the expected order of the adsorption; a weaker interaction is predicted for Na$^+$ than Rb$^+$. This discrepancy does not vary with the number of layers included in the cluster; however, it is eliminated by the use of a higher quality basis set: as is shown in Figure 4, using triple-ζ basis sets (def2-TZVP) gives the expected energetic order.[86]

As expected, correcting for the effect of BSSE on the adsorption energies (shown in brackets in Table I) generally decreases the strength of the interaction, and the magnitude of the counterpoise correction is smaller when higher quality basis sets are used; the energetic order between the ions is not altered.

To understand the effect of the surface representation on the adsorption energies, we looked at the adsorption of the same ions on three different surface models: a single layer, **6×6_1**, a surface containing a point charge layer underneath the QM cluster, **6×6_1+PC**, and a double layer with the same sized QM clusters in both, **6×6_2**. The relative adsorption energies were calculated by comparing the energies of the different systems to the original single layer results (see Table I). Including an extra PC layer (**6×6_1+PC**) results in a negligible difference in the adsorption energies. With def2-SVP basis
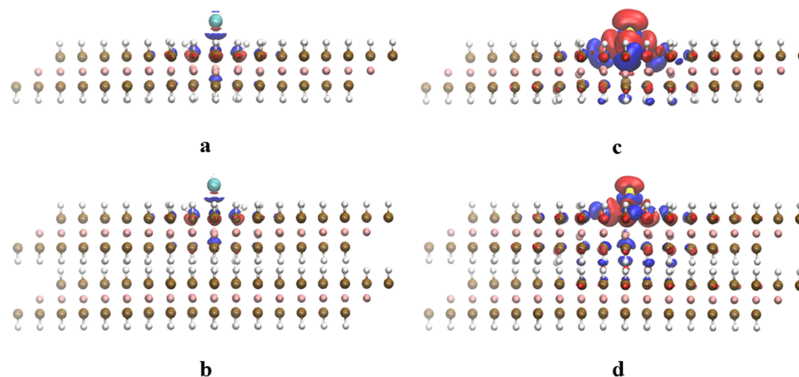

FIG. 3. Electron density difference plots of adsorbed Cs$^+$ ((a) and (b)) and Sr^{2+} ion ((c) and (d)) on **6×6_1** ((a) and (c)) and on **6×6_2** ((b) and (d)). The isosurface value was chosen to be 0.0025 a.u. throughout. The red regions are indicative of electron depletion, while the blue regions to electron accumulation. Point charges are not shown (Mg = pink, O = ochre, H = white, Sr = yellow, Cs = turquoise).[74]
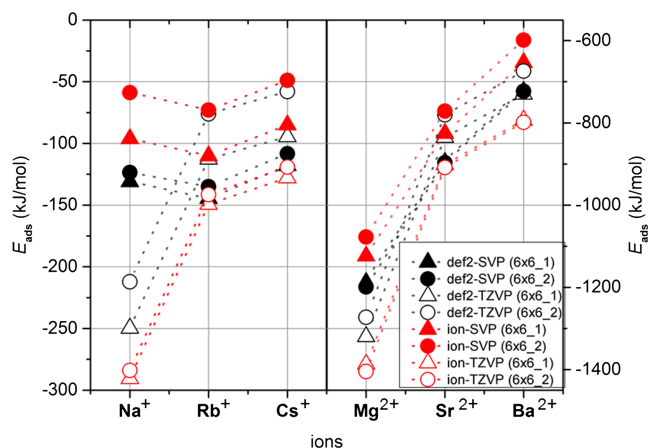
FIG. 4. Adsorption energies for a series of ions adsorbed on the **6×6_1** and **6×6_2** model surfaces, using different quality basis sets (def2-SVP, def2-TZVP or mixed basis sets).

sets, the ΔE_{ads} are c. 0.9 kJ/mol for Na$^+$, Rb$^+$ and Cs$^+$, while they are slightly larger (1.5-4.7 kJ/mol) for Mg^{2+}, Sr^{2+}, and Ba^{2+}. To place these differences in context, they are no more than ~0.7% of the original interaction energies in each case. These results suggest that the electrostatic contribution of the second layer to the ion/surface interaction is small.

Including the atoms of the second layer in the quantum chemically treated cluster (**6×6_2**) increases the dication adsorption energies slightly (except for Mg^{2+} due to its different behaviour compared to Sr^{2+} and Ba^{2+},[87] see the supplementary material, Figure (i)) but the opposite is true for the monocations, for which the energies decrease by 7.4-9.7 kJ/mol, 6%-8% of the actual adsorption energies. These values are in line with our previous suggestion based on Figure 3, i.e., that there is only a small electron donation from the second layer oxygen atoms in the case of Sr^{2+} and a negligible effect for Cs$^+$. We conclude that the adsorption of singly charged ions slightly distorts the positions of the second layer atoms, but with minimal polarisation; therefore, a quantum chemically treated second layer weakens the interactions overall.

A problem emerges when we use higher quality basis sets for the **6×6_2** systems. The relative adsorption energies with the def2-TZVP basis sets are ~36 kJ/mol for the monocations and ~55 kJ/mol for the dications. The significant shifts in energies, which are more than the 30% of the actual adsorption energies for the singly charged ions, are very likely the consequence of an artificial interaction. Larger basis sets might cause charge density increase closer to or overlapping the PC region leading to a falsely enhanced interaction. (The point charges were originally calculated with NPA in an iterative process using SVP quality basis sets for the QM cluster.) To probe this further, we explored a range of mixed basis set calculations. *Ion-TZVP* in Table I and Figure 4 indicates systems with the def2-SVP basis set on the surface atoms but def2-TZVP on the adsorbed ion and vice versa for *Ion-SVP*. Based on these results, we find that the deviation from the expected order in adsorption energies is clearly a function of basis set quality on the adsorbed ion, while the shift in the relative adsorption energies is related only to the basis sets of the surface atoms.

In summary, we conclude that our PEECM brucite model is capable of describing the energetics of ion/surface interactions, provided that sufficiently high quality basis sets are applied on the ions. Considering the surface as a two layered slab only slightly affects the adsorption energies, which suggests only a small contribution from the second layer atoms in the interaction.

B. Substitution of Ca^{2+} and Sr^{2+} into brucite

Our next study focussed on the energetics of substitution of heavier group II ions for Mg^{2+} in brucite, calculated with both the PEECM model and periodic DFT, using the same functional (PBE) and basis sets (Section II B) with the two different codes. We optimised structures with one (**6×6_1**) and two (**6×6_2**) layers included in the QM cluster for the PEECM model, excluding the **6×6_1+PC** surface representation which is not easily comparable with periodic DFT. We substituted each ion into the same position in the upper layer to avoid the possible effect of different relative positions related to the cluster boundaries. We considered four different supercell sizes with 1, 2, and 3 layers of brucite within the periodic DFT model. The following equation was used to calculate the substitution energy:

$$E_{sub} = \left(E_{brucite-M} + E_{Mg^{2+}} \right) - \left(E_{brucite-Mg} + E_{M^{2+}} \right), \quad (2)$$

where $E_{brucite-M}$ is the computed SCF energy of the optimised substituted structure, $E_{brucite-Mg}$ is the energy of the perfect brucite slab with the same surface representation as $E_{brucite-M}$, and $E_{Mg^{2+}}$ and $E_{M^{2+}}$ are the single point energies of the isolated ions.

The substitution energies are summarised in Table II. Both models yield the expected order based on the size of the ionic radii (72 pm (Mg^{2+}) < 95 pm (Ca^{2+}) < 118 pm (Sr^{2+})), i.e., the substitution of Ca^{2+} is less unfavoured than that for Sr^{2+}. If we compare the energies obtained with the largest (**9×9**) cell size in the periodic DFT calculations to the results of the isolated PEECM model, the two methods give reasonably similar results. Although the difference between them is not constant for the two ions, it is always less than c. 6% of the substitution energies. Including a 2nd layer of brucite in the surface model has only a slight effect on the substitution energy, which is interesting given that the substitution distorts the surface geometry much more than an adsorption reaction. The 2nd layer results in only a 2-6 kJ/mol difference in energy for each ion, irrespective of the method used.

TABLE II. Substitution energies (E_{sub}) calculated with periodic DFT and with the PEECM, including 1 or 2 explicit layers of brucite in the model. The energy differences between the two models are represented in percentages (E_{diff}) relative to the periodic DFT values.

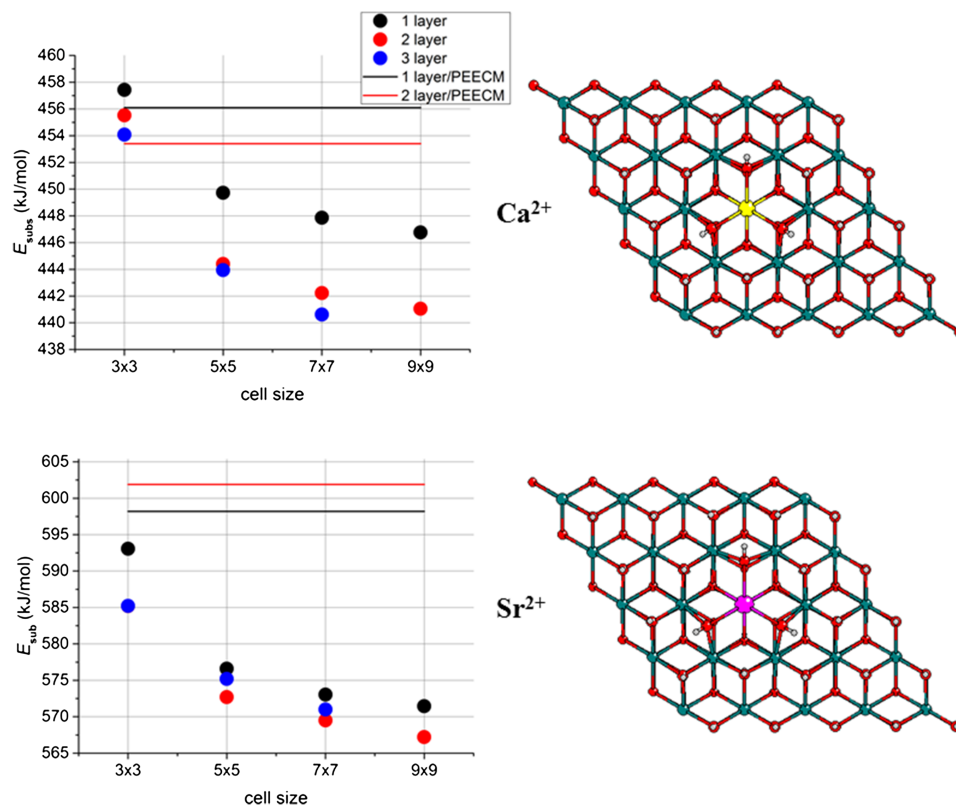| Surface models		Substitution energies			
		Ca^{2+}		Sr^{2+}	
Method	Layer	E_{sub}(kJ/mol)	E_{diff}(%)	E_{sub}(kJ/mol)	E_{diff}(%)
Periodic DFT	**9×9_1**	446.8		571.5	
PEECM	**6×6_1**	456.1	2.1	598.2	4.7
Periodic DFT	**9×9_2**	441.0		567.2	
PEECM	**6×6_2**	453.4	2.8	601.9	6.1

FIG. 5. Periodic DFT-calculated substitution energies as a function of cell size for systems containing 1, 2, or 3 brucite layers for Ca^{2+} and Sr^{2+}. Energies calculated for isolated systems in the PEECM method are represented with horizontal lines. Images are the optimised structures of substituted Ca^{2+} (yellow) and Sr^{2+} (magenta) into a **5×5_2** brucite cell (Mg = green, O = red, H = grey). Note that the gradient of the **7×7_3** system did not fully converge (the maximum gradient was 0.000 501 a.u. while the convergence criterion is 0.000 450), although the energy did.

The substitution energies as a function of cell size for different number of layers are plotted in Figure 5 (and summarised in supplementary material, Table (x)). With the use of bigger cell sizes in the periodic DFT model, the substitution energy converges, presumably towards the energy of a completely isolated interaction site. However, with cell sizes bigger than 3×3, the differences are small, 3-5 kJ/mol for each case, i.e., the effect of the substituted ion on the crystal structure is so localised that the ions are close to being isolated even with a 5×5 supercell. Adding a 2nd layer lowers the energy by 4-6 kJ/mol and including a 3rd layer has an even smaller effect on the energies.

This study of Ca^{2+} and Sr^{2+} substitution within a periodic DFT model suggests that moving from two- to three-layer slabs has little effect on substitution energies. This provides indirect evidence that the **6×6_2** QM cluster in the PEECM model includes all the necessary interactions and there is no need to increase the cluster size or the number of brucite layers in the QM region.

C. Adsorption of Sr[(OH)$_2$(H$_2$O)$_4$] on brucite

Our ultimate aim is to understand the interactions between hydrated brucite surfaces and solvated, fission-generated strontium. This study will involve many differently coordinated complexes and will use their relative energies to identify the most stable among them. Here we describe a first step towards this aim, i.e., an investigation of adsorbed Sr(OH)$_2$ complexes, surrounded by their first coordination

shell. [Sr(OH)$_2$(H$_2$O)$_4$] was chosen based on the most stable Sr^{2+} dihydroxide coordination with two solvation shells from our previous study.[58] We searched for the most stable structure of [Sr(OH)$_2$(H$_2$O)$_4$] adsorbed on brucite by placing it above the surface, and by generating three more initial structures via random rotation of the original molecule. We optimised the geometries in CRYSTAL, representing the brucite surface by a single layer 5×5 supercell slab (Figure 6). These optimised geometries were then used as starting structures in our TURBOMOLE simulations, where they were reoptimised with the PEECM model, placing each complex at the same initial position relative to the QM cluster.

We used an equation analogous to Eq. (1) in Section III A to calculate the adsorption energies (Table III), replacing the single point energy of a single ion with that of the solvated complex. There is an excellent agreement between the absolute adsorption energies obtained from the two methods: the energy difference is between 1.6% and 3.6% in each case with a single layer surface representation and 0.2%-4.0% for two-layered surface models. Structure **3** is predicted to be the most stable, and the relative adsorption energies (ΔE_{ads}) are calculated by comparing the energies of the other structures to that of structure **3**. The differences between the calculated relative energies are less than 2 kJ/mol using periodic DFT (**5×5** cell size) and the PEECM model for the single layer surface representation, with the exception of structure **4,** where the geometry of the optimised complexes differs between the two methods; therefore, there is a more significant energy
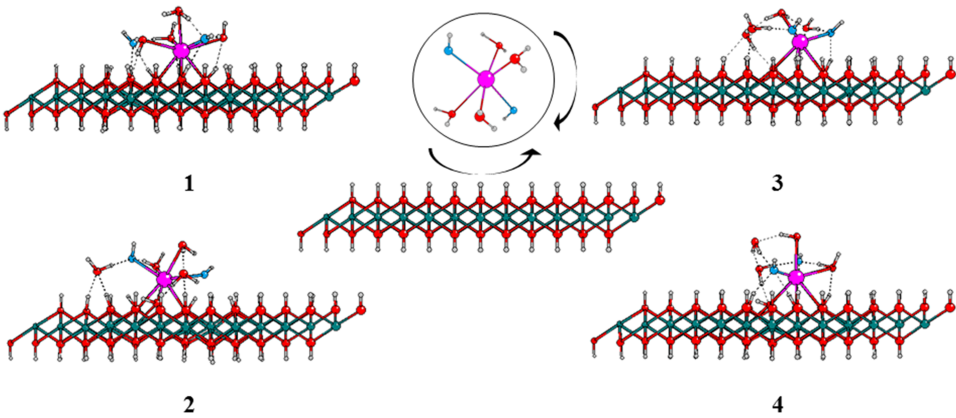
FIG. 6. *Middle*: The ball and stick representation of the *5×5_1* supercell and the original Sr(OH)$_2$ complex with its complete 1st coordination shell. *Side*: **1**, **2**, **3**, and **4** are the optimised structures of the adsorbed complexes with periodic DFT (Mg = green, O = red, H = grey, Sr = magenta, O in the coordinated OH groups = blue).

difference (8 kJ/mol). Increasing the cell size up to *7×7* and *9×9* in periodic DFT causes a less than 5 kJ/mol energy difference in the absolute adsorption energies. Although the values of the relative adsorption energy change more with bigger cell sizes compared with the excellent agreement shown for the *5×5* and *6×6* comparison, the energetic trend is not affected (the cell size study is shown in Section 4 of the supplementary material). This suggests that the *5×5* cell size is reasonable for periodic DFT and indirectly shows that the *6×6* cluster size used in the PEECM contains all the atoms in the QM region which play a part in the adsorption.

BSSE was considered and the counterpoise corrected values are presented in brackets in Table III. BSSE significantly decreases the absolute adsorption energies (by

c. 55-60 kJ/mol), but the relative energies are only slightly different from the uncorrected ones; this type of error largely cancels in the definition of the relative adsorption energy.[88]

When we consider a two-layer model in the PEECM, via either an extra PC layer (*6×6_1+PC*) or a second 6 × 6 cluster under the first (*6×6_2*), the relative adsorption energies are found to be very similar to the single layer results (*6×6_1*). Comparing ΔE_{ads} for *6×6_2* and *5×5_2* surface models, there are differences in relative adsorption energies in *5×5_2* compared to *5×5_1* due to minor structural differences affecting only water molecules which are not directly coordinated to the Sr^{2+} ion, but there is no change in terms of either energetic trends or coordination numbers.

TABLE III. Absolute (E_{ads}) and relative adsorption energies (ΔE_{ads}) of four Sr[(OH)$_2$(H$_2$O)$_4$] complexes, calculated by comparing each system to the most stable structure. Counterpoise corrected energy values are presented in brackets (BSSE).

		E_{ads} (kJ/mol)												
Structure		\multicolumn{3}{c	}{**1**}			\multicolumn{3}{c	}{**2**}			\multicolumn{3}{c	}{**3**}			\multicolumn{3}{c	}{**4**}
Coordination		\multicolumn{3}{c	}{CN = 8}			\multicolumn{3}{c	}{CN = 7-8}			\multicolumn{3}{c	}{CN = 6}			\multicolumn{3}{c	}{CN = 6-7}
Method	Layer	E	(BSSE)	E_{diff}(%)	E	(BSSE)	E_{diff}(%)	E	(BSSE)	E_{diff}(%)	E	(BSSE)	E_{diff}(%)
Periodic DFT	*5×5_1*	−431.7			−402.3			−444.4			−416.1		
PEECM	*6×6_1*	−422.7	(−366.7)	2.1	−393.8	(−332.7)	2.1	−437.2	(−380.2)	1.6	−401.1	(−349.2)	3.6
Periodic DFT	*5×5_2*	−428.4			−403.2			−438.6			−419.9		
PEECM	*6×6_2*	−424.6	(−371.2)	0.9	−391.8	(−332.4)	2.8	−439.6	(−384.3)	0.2	−403.3	(−353.0)	4.0
Periodic DFT	*5×5_2_f*	−430.1			−401.1			−435.9			−422.5		
PEECM	*6×6_2_f*	−411.3	(−358.2)	4.4	−379.9	(−320.8)	5.3	−428.0	(−372.9)	1.8	−391.4	(−341.1)	7.4

		ΔE_{ads} (kJ/mol)								
Method	Layer	E	(BSSE)	E	(BSSE)	E	(BSSE)	E	(BSSE)
Periodic DFT	*5×5_1*	12.7		42.1		0.0		28.2	
PEECM	*6×6_1*	14.5	(13.5)	43.4	(47.5)	0.0	(0.0)	36.1	(30.9)
Periodic DFT	*5×5_2*	10.2		35.4		0.0		18.7	
PEECM	*+PC*	14.2	(12.5)	49.0	(52.8)	0.0	(0.0)	34.0	(29.2)
PEECM	*6×6_2*	14.9	(13.2)	47.8	(51.9)	0.0	(0.0)	36.2	(31.3)
PEECM	*6×6_2_f*	16.7	(14.7)	48.1	(52.1)	0.0	(0.0)	36.6	(31.8)

TABLE IV. Sr–O distances (d) and electron densities at the bond critical points (ρ) for each coordinated OH group or H_2O molecule calculated with QTAIM for the optimised structures in PEECM or periodic DFT. For structures and Sr–O labels, see Figure 7.

| | 1 | | | | 2 | | | | 3 | | | | 4 | | | |
| | PEECM | | Periodic DFT | | PEECM | | Periodic DFT | | PEECM | | Periodic DFT | | PEECM | | Periodic DFT | |
Sr–O	d (Å)	ρ(a.u.)	d (Å)	ρ(a.u.)	d (Å)	ρ(a.u.)	d (Å)	ρ(a.u.)	d (Å)	ρ(a.u.)	d (Å)	ρ(a.u.)	d (Å)	ρ(a.u.)	d (Å)	ρ(a.u.)
Sr–OH(1)	2.710	0.0230	2.698	0.0234	2.630	0.0276	2.612	0.0285	2.680	0.0247	2.700	0.0236	2.685	0.0243	2.751	0.0210
Sr–OH(2)	2.572	0.0314	2.566	0.0318	2.562	0.0315	2.582	0.0306	2.629	0.0275	2.623	0.0277	2.602	0.0296	2.579	0.0310
Sr–OH(3)	2.564	0.0322	2.555	0.0327	2.760	0.0213	2.672	0.0252	2.595	0.0299	2.577	0.0309	2.567	0.0315	2.519	0.0355
Sr–OH(4)	2.553	0.0278	2.597	0.0253	2.481	0.0378	2.512	0.0365	2.422	0.0407	2.438	0.0399	2.427	0.0406	2.422	0.0419
Sr–OH(5)[a]	2.724	0.0217	2.783	0.0192	2.574	0.0294	2.579	0.0304	2.470	0.0375	2.495	0.0361	2.865	0.0133	3.072	0.0083
Sr–H_2O(1)	2.562	0.0311	2.583	0.0297	2.648	0.0274	2.642	0.0278	2.548	0.0336	2.574	0.0317	2.761	0.0205	2.853	0.0170
Sr–H_2O(2)	2.624	0.0284	2.644	0.0270	2.746	0.0202	2.793	0.0181	…	…	…	…	2.644	0.0278	2.595	0.0309
Sr–H_2O(3)	2.672	0.0255	2.695	0.0244	2.871	0.0153	3.331	…	…	…	…	…	2.941	0.0137	3.166	…
R^2	0.818		0.853		0.973		0.982		0.995		0.996		0.974		0.981	
Complex	[Sr(OH)$_4$(H$_2$O)$_4$]$^{2+}$				[Sr(OH)$_5$(H$_2$O)$_3$]$^{3+}$		[Sr(OH)$_5$(H$_2$O)$_2$]$^{3+}$		[Sr(OH)$_5$(H$_2$O)]$^{3+}$				[Sr(OH)$_5$(H$_2$O)$_3$]$^{3+}$		[Sr(OH)$_5$(H$_2$O)$_2$]$^{2+}$	
CN	8				8		7		6				8		7	

[a]In structure **1**, there is a fourth water coordinated to the Sr instead of a fifth OH group.

Freezing layers beneath the surface in a slab structure is a common approach to mimic the behaviour of the bulk underneath the top layer(s).[28] Although the biggest systems considered in this study contain only two-layered slabs, we calculated adsorption energies for surface representations in which the atomic positions in the second brucite layer are fixed (**6×6_2_f** and **5×5_2_f**) to study their possible effects on the adsorption. Turning to the periodic DFT results first, the adsorption energies for **5×5_2_f** are within ±2 kJ/mol of to the **5×5_2** results, i.e. fixing the atomic positions has no significant effect on the structures. In the case of the **6×6_2_f** PEECM model, E_{ads} is ~12 kJ/mol higher than the adsorption energies of **6×6_2**. Since comparing the optimised geometries did not reveal changes in the adsorbed structures, we surmise that this constant energy shift is probably due to the fact that, in addition to using constraints within the QM cluster, we used

the experimental crystal parameters for the PEECM surface, while the crystal parameters were previously optimised for the bulk mineral structure in periodic DFT. But despite the less accurate crystal structure description in the embedded methods, ΔE_{ads} values are not affected by changes in the second layer, as shown in Table III: energies for **6×6_2_f** are very close to the **6×6_1** and **6×6_2** results.

Overall, this study suggests that including a relaxed or fixed 2nd layer in the surface model has only minor effects on the relatively weak adsorptions of the hydrated complexes. While there are some small differences in relative adsorption energies, the energetic trends within structures **1**-**4** and the geometries of the coordinated Sr^{2+} complexes do not change. Results obtained from periodic DFT and PEECM predict similar structures and have the same energetic trends.
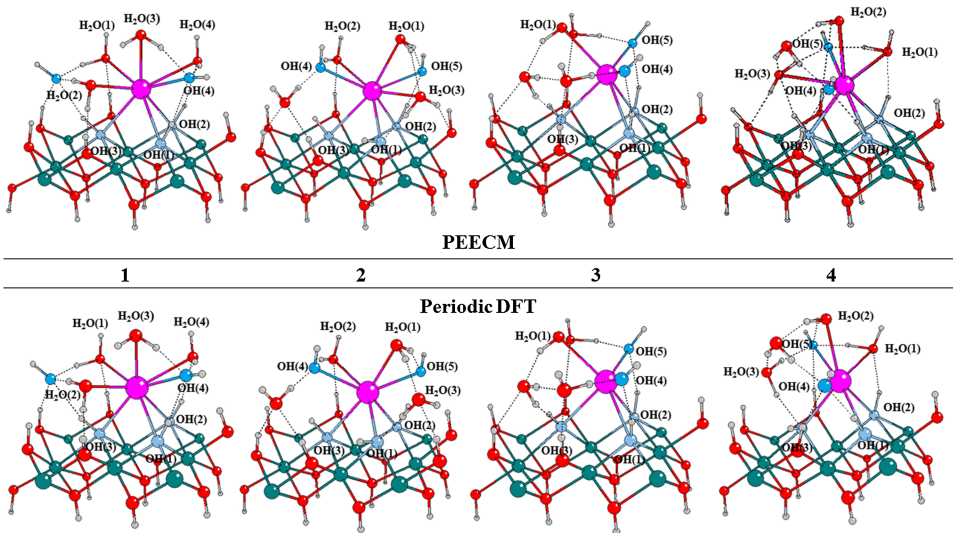

FIG. 7. The optimised geometries of structures **1-4** in PEECM or periodic DFT. The coordinated H_2O molecules and OH groups are labelled according to Table IV (Mg = green, O = red, H = grey, Sr = magenta, O in the coordinated OH ion = dark blue, O in the coordinated OH groups of the surface = light blue).
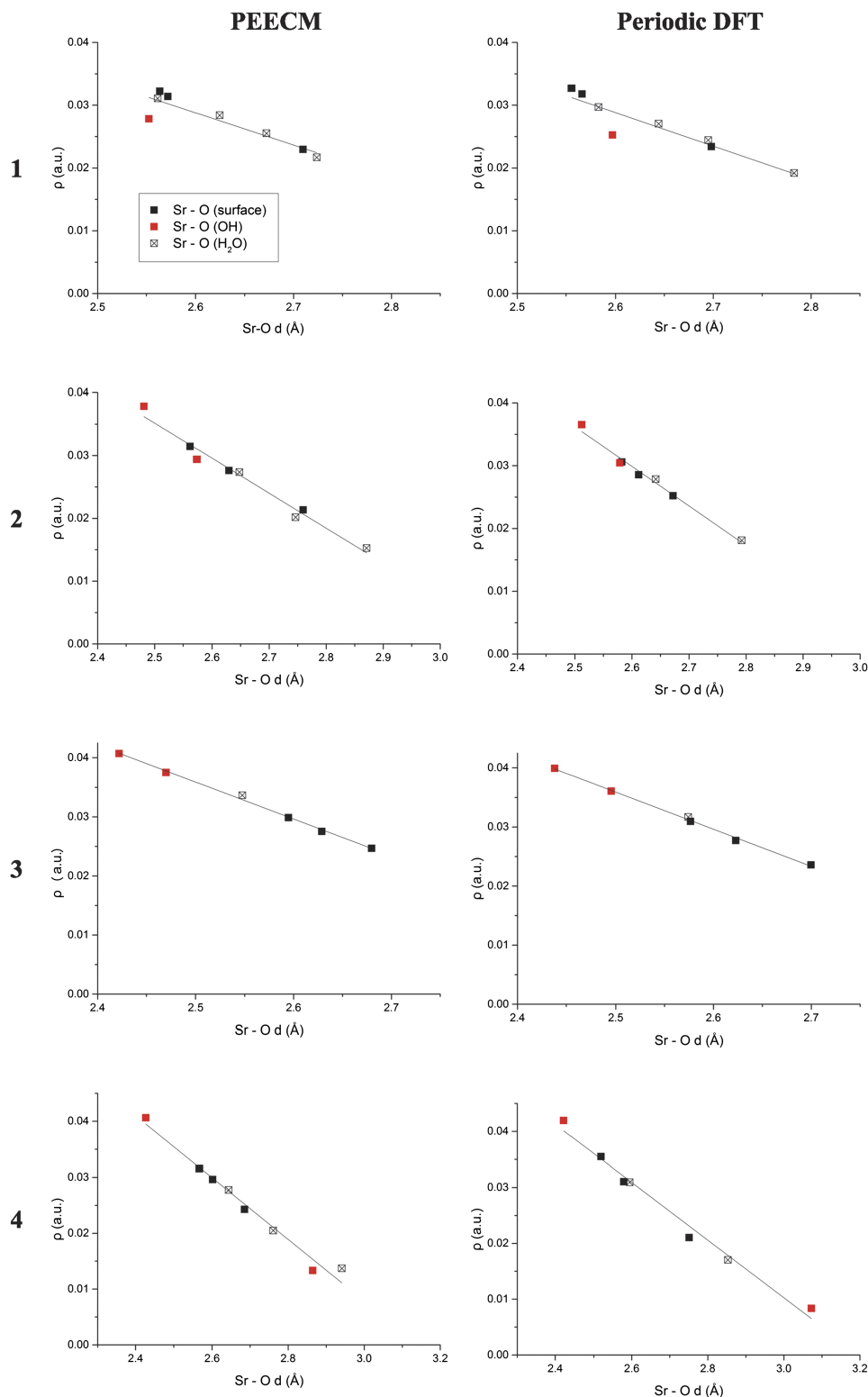
FIG. 8. Electron densities at the Sr–O BCPs plotted against Sr–O distances for the four $Sr[(OH)_2(H_2O)_4]$ complexes optimised with PEECM or periodic DFT. Red squares are related to the Sr–O(OH) interactions in the solvation shell, crossed squares to the Sr–O(H_2O) interactions in the solvation shell, and black squares to the Sr–O(surface) interactions with the surface OH groups.

1. Assessment of local coordination via the QTAIM

In order to probe further the comparison between the periodic DFT- and the PEECM-generated structures, we explored the coordination environment around the Sr^{2+} ion by examining the Sr–O distances and by calculating QTAIM

bond critical point (BCP) electron densities for the Sr–O interactions (Table IV). The QTAIM is a well-known theory which uses the topology of the electron density to analyse atomic properties in molecules or complexes.[89,90] Bond critical points are stationary points in the electron density distribution where the minimum along the path of maximum

electron density between two nuclei is found at the interatomic surface. The electron density at the BCPs is often related to the strength of the interaction,[91,92] with higher values indicating stronger bonds.

The final structures obtained with the two different methods are found to be generally very similar by topological analysis. The coordination environment of the Sr is almost the same in complexes **1** and **3**, although there is a slight difference in structure **2**, in which the $H_2O(3)$ water molecule (see structure **2** in Figure 7) is predicted to be very weakly coordinated to the Sr in the PEECM ($\rho = 0.0153$ a.u.), while there is no similar interaction between the Sr and that water molecule in the periodic DFT model. Defining coordination to be the presence of a Sr–O BCP, we conclude that the overall coordination number (CN) in complex **2** is 8 with PEECM and 7 with periodic DFT. The difference in the geometry of structure **4** is more significant (Figure 7); due to the different orientation of the $H_2O(3)$ water molecule in the embedded model, it is weakly coordinated to the Sr ($d = 2.941$ Å, $\rho = 0.0137$ a.u.) and it also modifies the strength of the other coordinated ligands, e.g., OH(5) has a shorter Sr–O distance (2.865 Å) and higher electron density at the BCP (0.0133 a.u.) in the PEECM geometry than in the final structure of periodic DFT (3.072 Å, 0.0083 a.u.).

Previous studies predict a generally good correlation between BCP electron densities and related bond lengths[92–94] and indeed, plotting the electron densities at the BCPs against the Sr–O distances (Figure 8) reveals a strong correlation between the two properties (calculated R^2 values for the linear regression are summarised in Table IV) and also illustrates the similarity in coordination between analogous structures calculated with PEECM and periodic DFT. There are three types of Sr–O interactions, based on the type of the coordinating oxygen atom: O of the OH⁻ ions in the solvation shell, surface OH groups (referred as O(OH) and O(surface) in the following text) and H_2O molecules in the solvation shell (O(H_2O)). The ones expected to have the strongest interaction with the Sr^{2+} ion are the OH⁻ ions in the solvation shell. However, this is not always the case, in fact, in structure **1** the only OH⁻ ion directly coordinating to the Sr is slightly outstanding from the trend, resulting in an R^2 value of 0.818 (0.853) with PEECM (periodic DFT). The O(OH) in this case has a weaker interaction according to the QTAIM analysis than the Sr–O distance would suggest, but the reason for this behaviour is unknown. Furthermore, in structure **4**, there is a very weakly coordinated O(OH) in the complex (OH(5)), as opposed to the other OH ion, OH(4), which has the strongest coordination to the Sr ion. In structure **3**, which is predicted to be the most stable, the OH⁻ ions in the solvation shell have the strongest interaction, followed by the only coordinated water molecule and then the surface OH groups which exhibit the weakest interaction.

IV. CONCLUSIONS

The PEECM has been used for the first time to model a layered, not purely ionic surface (brucite (0001)) and the developed model has been tested in three studies related to our final goal, studying the adsorption of radioactive ions on hydrated brucite surfaces.

The PEECM is capable of describing the adsorption of single s block ions onto brucite, although the basis set quality has to be carefully considered. At least triple-zeta quality is necessary to obtain the correct energetic ordering between the ions, but these larger basis functions must be avoided in the QM representation of the surface cluster, since they can cause artificial interactions between the boundary atoms and the point charge region.

Through a comparison with periodic DFT, we have demonstrated that the PEECM sufficiently reflects the qualities of the brucite surface to be able to describe both the substitution of Ca^{2+} or Sr^{2+} into brucite and the surface complexation of $[Sr(OH)_2(H_2O)_4]$. Based on the cell size studies and the interaction energies obtained with multiple layers of brucite, the size of the quantum chemically treated cluster is found to be reasonable in all cases. The agreement between adsorption energies and the optimised geometries obtained with PEECM or periodic DFT is excellent in the case of the adsorption of $[Sr(OH)_2(H_2O)_4]$ complexes.

These results give us confidence in using the embedded brucite (0001) model in future investigations of Sr^{2+} and Cs^+ complex ion adsorptions on hydrated surfaces. They demonstrate that the PEECM is capable of describing sorption mechanisms on brucite-like surfaces, and that the approach is a viable alternative to periodic DFT when ionic species are involved in surface interactions. Furthermore, we note that the PEECM calculations presented here were run largely on our local departmental compute server, with a modest number of cores per calculation, by contrast to the periodic DFT calculations, which required the massively parallel version of the CRYSTAL code and were run on the UK's national supercomputing facility.

We are currently extending our PEECM study to include many more water molecules in the QM region to probe effects of second shell water molecules on the adsorption, and the results of this will be presented in a forthcoming paper.

SUPPLEMENTARY MATERIAL

See supplementary material for information such as the validation of the surface models with PEECM and periodic DFT, basis set comparison for the adsorption of s block ions, and the cell size study for the $Sr[(OH)_2(H_2O)_4]$ complexes with periodic DFT.

ACKNOWLEDGMENTS

the Research Computing "Legion" cluster (Legion@UCL) and associated services.

[1] S. Chrétien and H. Metiu, J. Chem. Phys. **126**, 104701 (2007).

[2] S. A. Fuente, C. A. Ferretti, N. F. Domancich, V. K. Díez, C. R. Apesteguía, J. I. Di Cosimo, R. M. Ferullo, and N. J. Castellani, Appl. Surf. Sci. **327**, 268 (2015).

[3] S. Rangarajan and M. Mavrikakis, ACS Catal. **6**, 2904 (2016).

[4] J. R. B. Gomes and J. A. N. F. Gomes, J. Electroanal. Chem. **483**, 180 (2000).

[5] X.-Y. Pang, C. Wang, Y.-H. Zhou, J.-M. Zhao, and G.-C. Wang, J. Mol. Struct.: THEOCHEM **948**, 1 (2010).

[6] D. Costa, P.-A. Garrain, and M. Baaden, J. Biomed. Mater. Res., Part A **101A**, 1210 (2013).

[7] S. Kerisit, P. Zarzycki, and K. M. Rosso, J. Phys. Chem. C **119**, 9242 (2015).

[8] J. Setiadi, M. D. Arnold, and M. J. Ford, ACS Appl. Mater. Interfaces **5**, 10690 (2013).

[9] H. Weber, T. Bredow, and B. Kirchner, J. Phys. Chem. C **119**, 15137 (2015).

[10] M. P. Andersson, H. Sakuma, and S. L. S. Stipp, Langmuir **30**, 6129 (2014).

[11] J. A. Greathouse, R. J. O'Brien, G. Bemis, and R. T. Pabalan, J. Phys. Chem. B **106**, 1646 (2002).

[12] J. D. Kubicki, K. D. Kwon, K. W. Paul, and D. L. Sparks, Eur. J. Soil Sci. **58**, 932 (2007).

[13] S. Lectez, J. Roques, M. Salanne, and E. Simoni, J. Chem. Phys. **137**, 154705 (2012).

[14] E. Veilly, J. Roques, M.-C. Jodin-Caumon, B. Humbert, R. Drot, and E. Simoni, J. Chem. Phys. **129**, 244704 (2008).

[15] S. E. Mason, C. R. Iceman, K. S. Tanwar, T. P. Trainor, and A. M. Chaka, J. Phys. Chem. C **113**, 2159 (2009).

[16] S. E. Mason, T. P. Trainor, and A. M. Chaka, J. Phys. Chem. C **115**, 4008 (2011).

[17] K. W. Corum and S. E. Mason, Mol. Simul. **41**, 146 (2015).

[18] S. Yang, C. Chen, Y. Chen, J. Li, D. Wang, X. Wang, and W. Hu, ChemPlusChem **80**, 480 (2015).

[19] S. K. Ramadugu and S. E. Mason, J. Phys. Chem. C **119**, 18149 (2015).

[20] G. García, M. Atilhan, and S. Aparicio, Phys. Chem. Chem. Phys. **17**, 16315 (2015).

[21] R. Dovesi, B. Civalleri, R. Orlando, C. Roetti, V. R. Saunders, in *Reviews in Computational Chemistry*, edited by K. B. Lipkowitz, R. Larter, and T. R. Cundari (Wiley-VCH, 2005).

[22] G. Pacchioni, J. Chem. Phys. **128**, 182505 (2008).

[23] V. Ballenegger, A. Arnold, and J. J. Cerdà, J. Chem. Phys. **131**, 094107 (2009).

[24] S. C. Ammal and A. Heyden, J. Chem. Phys. **133**, 164703 (2010).

[25] J. Carrasco, N. Lopez, F. Illas, and H.-J. Freund, J. Chem. Phys. **125**, 074711 (2006).

[26] C. A. Gilbert, R. Smith, and S. D. Kenny, Nucl. Instrum. Methods Phys. Res., Sect. B **255**, 166 (2007).

[27] A. M. Burow, M. Sierka, J. Döbler, and J. Sauer, J. Chem. Phys. **130**, 174710 (2009).

[28] A. V. Bandura, D. G. Sykes, V. Shapovalov, T. N. Troung, J. D. Kubicki, and R. A. Evarestov, J. Phys. Chem. B **108**, 7844 (2004).

[29] B. Herschend, M. Baudin, and K. Hermansson, Chem. Phys. **328**, 345 (2006).

[30] J. L. F. Da Silva, M. V. Ganduglia-Pirovano, J. Sauer, V. Bayer, and G. Kresse, Phys. Rev. B **75**, 045121 (2007).

[31] TURBOMOLE Version 6.5 User's Manual, Program Package for *ab initio* Electronic Structure Calculations, 2012, pp. 132–139.

[32] K. N. Kudin and G. E. Scuseria, Chem. Phys. Lett. **283**, 61 (1998).

[33] Sellafield Ltd., Sellafield Integrated Waste Strategy Version 2 Report and Recommendations, 2007.

[34] C. R. Gregson, D. T. Goddard, M. J. Sarsfield, and R. J. Taylor, J. Nucl. Mater. **412**, 145 (2011).

[35] S. Owens, M. Higgins-Bos, M. Bankhead, and J. Austin, NNL Sci. (3), 4 (2015).

[36] X. Tan, M. Fang, and X. Wang, Molecules **15**, 8431 (2010).

[37] T. Hattori, T. Saito, K. Ishida, A. C. Scheinost, T. Tsuneda, S. Nagasaki, and S. Tanaka, Geochim. Cosmochim. Acta **73**, 5975 (2009).

[38] A. Kremleva, S. Krüger, and N. Rösch, J. Phys. Chem. C **120**, 324 (2016).

[39] F. M. Higgins, N. H. de Leeuw, and S. C. Parker, J. Mater. Chem. **12**, 124 (2002).

[40] M. Johnson, D. O'Connor, P. Barnes, C. R. A. Catlow, S. L. Owens, G. Sankar, R. Bell, S. J. Teat, and R. Stephenson, J. Phys. Chem. B **107**, 942 (2003).

[41] M. Catti, G. Ferraris, S. Hull, and A. Pavese, Phys. Chem. Miner. **22**, 200 (1995).

[42] F. Zigan and R. Rothbauer, Neues Jahrb. Fuer Miner. Monatshefte **4**, 137 (1967).

[43] R. LeSar and R. G. Gordon, Phys. Rev. B **25**, 7221 (1982).

[44] P. D'Arco, M. Causà, C. Roetti, and B. Silvi, Phys. Rev. B **47**, 3522 (1993).

[45] B. Winkler, V. Milman, B. Hennion, M. C. Payne, M.-H. Lee, and J. S. Lin, Phys. Chem. Miner. **22**, 461 (1995).

[46] P. Baranek, A. Lichanot, R. Orlando, and R. Dovesi, Chem. Phys. Lett. **340**, 362 (2001).

[47] F. Pascale, S. Tosoni, C. Zicovich-Wilson, P. Ugliengo, R. Orlando, and R. Dovesi, Chem. Phys. Lett. **396**, 308 (2004).

[48] P. Ugliengo, C. M. Zicovich-Wilson, S. Tosoni, and B. Civalleri, J. Mater. Chem. **19**, 2564 (2009).

[49] K. Azuma, T. Oda, and S. Tanaka, Comput. Theor. Chem. **963**, 215 (2011).

[50] A. M. Chaka and A. R. Felmy, J. Phys. Chem. A **118**, 7469 (2014).

[51] M. B. Kruger, Q. Williams, and R. Jeanloz, J. Chem. Phys. **91**, 5910 (1989).

[52] D. E. Haycock, M. Kasrai, C. J. Nicholls, and D. S. Urch, J. Chem. Soc. Dalton. Trans. **12**, 1791 (1978).

[53] J. D. Bernal and H. D. Megaw, Proc. R. Soc. A **151**, 384 (1935).

[54] G. Wulff, Zeitschrift Fur Kryst. Und Mineral **34**, 449 (1901).

[55] M. R. Carrott, P. Carrott, M. B. de Carvalho, and K. S. W. Sing, J. Chem. Soc. Faraday Trans. **87**, 185 (1991).

[56] A. Kerridge and N. Kaltsoyannis, Chem. - Eur. J. **17**, 5060 (2011).

[57] A. Kerridge and N. Kaltsoyannis, Dalton Trans. **40**, 11258 (2011).

[58] E. Makkos, A. Kerridge, and N. Kaltsoyannis, Dalton Trans. **44**, 11572 (2015).

[59] E. H. Teunissen, A. P. J. Jansen, R. A. van Santen, R. Orlando, and R. Dovesi, J. Chem. Phys. **101**, 5865 (1994).

[60] J. M. Vollmer, E. V Stefanovich, and T. N. Truong, J. Phys. Chem. B **103**, 9415 (1999).

[61] TURBOMOLE V6.6 2014, a Development of University of Karlsruhe and Forschungszentrum Karlsruhe GmbH, 1989-2007, TURBOMOLE GmbH since 2007, available from http://www.turbomole.com.

[62] K. Eichkorn, O. Treutler, H. Öhm, M. Häser, and R. Ahlrichs, Chem. Phys. Lett. **242**, 652 (1995).

[63] P. Ugliengo, G. Borzani, and D. Viterbo, J. Appl. Crystallogr. **21**, 75 (1988).

[64] J. Tao, J. P. Perdew, V. N. Staroverov, and G. E. Scuseria, Phys. Rev. Lett. **91**, 146401 (2003).

[65] A. Schäfer, H. Horn, and R. Ahlrichs, J. Chem. Phys. **97**, 2571 (1992).

[66] K. Eichkorn, F. Weigend, O. Treutler, and R. Ahlrichs, Theor. Chem. Acc. **97**, 119 (1997).

[67] For the *6×6_1+PC* surface representation, the lower hydrogen atoms were also constrained during optimisation.

[68] J. P. W. Wellington, A. Kerridge, and N. Kaltsoyannis, Polyhedron **116**, 57 (2016).

[69] A. E. Reed, R. B. Weinstock, and F. Weinhold, J. Chem. Phys. **83**, 735 (1985).

[70] F. Weigend and R. Ahlrichs, Phys. Chem. Chem. Phys. **7**, 3297 (2005).

[71] M. Kaupp, P. v R. Schleyer, H. Stoll, and H. Preuss, J. Chem. Phys. **94**, 1360 (1991).

[72] W. Zou, D. Nori-Shargh, and J. E. Boggs, J. Phys. Chem. A **117**, 207 (2013).

[73] T. Lu and F. Chen, J. Comput. Chem. **33**, 580 (2012).

[74] This Image Was Made with VMD Software Support. VMD Is Developed with NIH Support by the Theoretical and Computational Biophysics Group at the Beckman Institute, University of Illinois at Urbana-Champaign. www.ks.uiuc.edu/.

[75] T. A. Keith, AIMALL (Version 13.11.04); T. A. Keith, TK Gristmill Software, Overl. Park, KS, USA, (aim.tkgristmill.com) (2013).

[76] R. Dovesi, V. R. Saunders, C. Roetti, R. Orlando, C. M. Zicovich-Wilson, F. Pascale, B. Civalleri, K. Doll, N. M. Harrison, I. J. Bush, P. D'Arco, M. Llunell, M. Causà, and Y. Noël, *CRYSTAL14 User's Manual* (University of Torino, Torino, 2014).

[77] R. Dovesi, R. Orlando, A. Erba, C. M. Zicovich-Wilson, B. Civalleri, S. Casassa, L. Maschio, M. Ferrabone, M. De La Pierre, P. D'Arco, Y. Noël, M. Causà, M. Rérat, and B. Kirtman, Int. J. Quantum Chem. **114**, 1287 (2014).

[78] J. P. Perdew, K. Burke, and M. Ernzerhof, Phys. Rev. Lett. **77**, 3865 (1996).

[79] S. Grimme, J. Antony, S. Ehrlich, and H. Krieg, J. Chem. Phys. **132**, 154104 (2010).

[80]S. Grimme, J. Comput. Chem. **27**, 1787 (2006).

[81]M. F. Peintinger, D. V. Oliveira, and T. Bredow, J. Comput. Chem. **34**, 451 (2013).

[82]A. Erba, K. E. El-Kelany, M. Ferrero, I. Baraille, and M. Rérat, Phys. Rev. B **88**, 035102 (2013).

[83]J. L. F. Da Silva, C. Stampfl, and M. Scheffler, Surf. Sci. **600**, 703 (2006).

[84]Since we were using the same computational parameters, the calculated energies were essentially the same for isolated systems in vacuum with both CRYSTAL14 and TURBOMOLE with less than 10^{-6} a.u. difference.

[85]S. F. Boys and F. Bernardi, Mol. Phys. **19**, 553 (1970).

[86]We explored further the effect of higher quality basis sets by using def2-QZVP for test calculations on single layered systems and found that the use of quadruple-ζ basis sets seemed to result in only a constant shift in adsorption energies when compared to triple-ζ results. (see supplementary material, Table (ix)).

[87]Magnesium adsorption effectively incorporates an extra Mg ion into the $Mg(OH)_2$ crystal structure; the ion-surface distance is much smaller in this case and the interaction much stronger, see supplementary material Figure (i).

[88]We did not calculate the BSSE in CRYSTAL since it largely depends on the geometry and the basis functions employed, both of which are almost the same in the two methods. Hence we expect the BSSE to be very similar in the two models. Besides, the relative adsorption energies, in which we are primarily interested, are largely unaffected by this type of error.

[89]C. F. Matta and R. J. Boyd, "An introduction to the quantum theory of atoms in molecules," in *The Quantum Theory of Atoms in Molecules: From Solid State to DNA and Drug Design* (WILEY-VCH Verlag GmbH & Co. KGaA, Weinheim, 2007).

[90]R. F. W. Bader, *Atoms in Molecules: A Quantum Theory* (Oxford University Press, New York, 1990).

[91]A. R. E. Mountain and N. Kaltsoyannis, Dalton. Trans. **42**, 13477 (2013).

[92]S. J. Grabowski, J. Phys. Org. Chem. **17**, 18 (2004).

[93]B. Bankiewicz, P. Matczak, and M. Palusiak, J. Phys. Chem. A **116**, 452 (2012).

[94]I. Alkorta, I. Rozas, and J. Elguero, Struct. Chem. **9**, 243 (1998).